On the pH-dependence of α-synuclein amyloid polymorphism and the role of secondary nucleation in seeding experiments

Lukas Frey[1†], Dhiman Ghosh[1†], Bilal M. Quereshi[2†], David Rhyner[1], Ricardo Guerrero-Ferreira[3] Aditya Pokharna[1], Witek Kwiatkowski[1], Tetjana Serdiuk[4], Paola Picotti[4], Roland Riek[1,*], Jason Greenwald[1,*]

[1]Institute of Molecular Physical Science, Vladimir-Prelog-Weg 2, ETH Zürich, Zürich, Switzerland
[2]Scientific Center for Optical and Electron Microscopy, Otto-Stern-Weg 3, ETH Zürich, Zürich, Switzerland
[3]Laboratory of Biological Electron Microscopy, Route de la Sorge, EPFL Lausanne, Lausanne, Switzerland

[4]Institute of Molecular Systems Biology, ETH Zürich, Zürich, Switzerland

[†]These authors contributed equally to this work

Keywords: amyloids, Parkinson's disease, α-synuclein, polymorphism

*Correspondence to: roland.riek@phys.chem.ethz.ch; jason.greenwald@phys.chem.ethz.ch

Abstract
The aggregation of the protein alpha-synuclein is closely associated with several neurodegenerative disorders and as such the structures of the amyloid fibril aggregates have high scientific and medical significance. However, it seems that there are about as many unique atomic-resolution structures of these aggregates as there are publications describing them. Obviously, this highly polymorphic nature of alpha-synuclein fibrils hampers efforts in disease-relevant *in vitro* studies on alpha-synuclein amyloid aggregation. In order to better understand the factors that affect polymorph selection we studied the structures of alpha-synuclein fibrils *in vitro* as a function of pH and buffer using cryo-EM helical reconstruction. We find that in the physiological range of pH 5.8-7.4 a pH-dependent selection between Types 1, 2 and 3 polymorphs occurs. Our results indicate that even in the presence of seeds, the polymorph selection during aggregation is highly dependent on the buffer conditions, attributed to the polymorph-unspecific nature of secondary nucleation. We also uncovered two new polymorphs that occur at pH 7.0 in phosphate buffered saline. The first is a monomeric Type 1 which highly resembles the structure of the juvenile-onset synucleinopathy polymorph found in patient-derived material. The second is a new Type 5 polymorph that resembles a polymorph that has been recently reported in a study that used diseased tissues to seed aggregation. Taken together, our results highlight the shallow amyloid energy hypersurface that can be altered by subtle changes in the environment, including the pH which is shown to play a major role in polymorph selection and in many cases appears to be the determining factor in seeded aggregation. The results also confirm the possibility of producing disease relevant structure *in vitro*.

Introduction

Amyloid fibrils are a unique class of self-assembled filamentous protein/peptide aggregates that historically have been associated with dozens of human diseases including Alzheimer's, Parkinson's, type II diabetes, and prion diseases[1]. It has long been understood that all amyloids contain a common structural scaffold known as the cross β-sheet motif, yet only more recently, with the advent of solid-state nuclear magnetic resonance spectroscopy (NMR)[2] and cryo-electron microscopy (cryo-EM) helical reconstruction[3], has it become clear that this shared repetitive motif can generate a wide range of structural folds[4,5]. Yet unlike globular proteins, whose amino acid sequence typically guides the protein folding process into a unique 3-dimensional structure, the amyloid structures derived from a single peptide sequence are often polymorphic: they can exist in various stable three-dimensional architectures. Another unique property of amyloids is their tendency to induce their own formation in a self-replicative manner. Amyloid formation is a nucleated growth process analogous to the growth of a 1D crystal[6] and can therefore be kinetically enhanced and spread by seeds. In seeding, the amyloid itself acts as a structural template for nucleation and growth, thereby inducing protein monomers into the amyloid fold resulting in fibril elongation. Additionally, as revealed by kinetic experiments, there appears to be the presence of secondary nucleation, which includes de novo seed formation on the side surface of the amyloid fibrils[7]. Structural polymorphism and seeding-enhanced growth are two hallmarks of amyloid biology. However, despite their likely importance in the etiology of many diseases, the factors that control polymorphs and the molecular mechanisms of seeding are poorly understood.

Amyloid polymorphs with differences large or small in both the tertiary structure (the arrangement of the β-strands) and the quaternary structure (protofilament-protofilament assembly) have been found to display distinct biological activities[8]. In the case of the protein tau, cryo-EM has been used to correlate 14 different tauopathies with distinct combinations of 8 different amyloid polymorphs[9,10]. In the case of α-synuclein (α-Syn), the structures of many *in vitro* polymorphs have been determined[11–34] yet they are all distinct from the polymorphs that have been extracted from the brains of patients of both multiple systems atrophy (MSA)[21] and Parkinson's disease (PD)[31]. Understanding how these disease-relevant polymorphs form

and reproducing them in vitro will be critical in the study of these synucleinopathies. Some clues are present in the brain-derived structures: two MSA polymorphs contain an unidentified molecule at the interface of the two protofilaments and in the PD polymorph an unidentified molecule appears to be stabilizing the structure of the fibril monomer. These findings support the idea that the environment plays a critical role in amyloid formation, essentially dictating which polymorphs are accessible and that the polymorph type is in some way associated with the disease.

Concerning the seeding of polymorphs, it was demonstrated that prion strains with their specific pathologies can be serially transmitted from animal to animal[35,36] and that strains can be amplified *in vitro* by the so-called protein misfolding amplification assay (PMCA)[37,38] or similar approaches[39]. However, *in vitro,* amyloid seeding is not always 100% faithful in reproducing the seed polymorph. In the case of α-Syn, PMCA-based seeding has been proposed as a diagnostic tool that could also differentiate between MSA and PD[38,40]. However, attempts to amplify the MSA and the PD patient-derived polymorphs *in vitro* with recombinant α-Syn have thus far failed[26,41,42]. Such failures might be attributed to the strong role of secondary nucleation in α-Syn aggregation, whereby the polymorph structure is not transmitted due to the flexible nature of the interactions involved in α-Syn secondary nucleation[43] so that environmental factors play a larger role in polymorph selection[26].

Seeding with α-Syn disease-derived amyloids does produce several amyloid polymorphs at low α-Syn concentrations (where no amyloids form without seeding), yet none of them was the same polymorph as that of the seeds[26]. In contrast, seeding experiments with *in vitro*-derived polymorphs have yielded mixed results whereby some polymorphs are seemingly easier to reproduce via seeding than others (such as Type 4 polymorph from E46K[22] or G51D[23] mutants) while using very high seed concentrations (10%) and by limiting primary and secondary nucleation processes, a polymorph that forms normally only at low salt can be produced at high salt and vice versa[44,45].

Having observed the plethora of α-Syn fibril polymorphs published in just the last few years, we set out to investigate the relationship between α-Syn polymorphs and their aggregation conditions. The speed and abundance of polymorphs being discovered have led to inconsistent naming conventions, and in this work, we expand upon previous nomenclature[13,19] which is illustrated in Figure 1, whereby polymorphs with distinct folds are assigned different Arabic numerals and sub-polymorphs formed through different proto-filament interfaces given different letters (with the exception of polymorph 1B whose name is kept for consistency with previous publications despite itself being a distinct fold, see Figure 2). We find that the pH of the aggregation condition is a major but not the only factor in determining which polymorph is formed *in vitro*. While attempting to reproduce the published conditions for the Type 2 polymorph, we found both a new polymorph (here termed Type 5) and produced a monomeric Type 1 polymorph, providing further evidence that the energetic landscape of α-Syn aggregation is rough with many interconnected local minima. In addition, our findings with cross-pH seeding experiments support the notion that seeding with α-Syn is non-polymorph-specific under conditions of secondary nucleation-dominated aggregation[44], consistent with the failure to recreate the *in-vivo* observed fibrils through seeding[26].

Results and Discussion

The range of accessible polymorphs is controlled by pH

There are more than 60 *in vitro* amyloid structures of α-Syn deposited in the PDB, representing over a dozen different structural polymorphs. The authors of these structures often try to frame newly observed polymorph(s) in the context of the diseases associated with α-Syn aggregation. However, given so many published structures, an examination of the conditions under which the polymorphs were formed also offers hints into the environmental influences of polymorph selection. In particular, we noted that Type 1 structures were observed almost

exclusively above pH 7.0, while Type 2 and 3 structures were observed below pH 7.4 and down to pH 6.5. To systematically analyze the effect of buffer and pH we studied the structures of α-Syn amyloids of the full-length, N-terminally acetylated protein grown under a variety of conditions. In a first series, we produced α-Syn amyloids in PBS (10 mM PO_4, 137 mM NaCl, 2.7 mM KCl) at the physiological pH values of 7.4, 7.0, 6.5, and 5.8.

At pH 5.8 we observed exclusively the Type 3 structures 3B and 3C (Figures 3 and 4). Considering the similarities between Type 2 and 3 structures (see below), it is noteworthy that a 2A-like polymorph was never observed for Type 3. In its place, we find the 3C polymorph for which the contacts are shifted by one residue with respect to 2A and are now defined by a salt bridge between E46 and K58 instead of K45 and E57. In the previously reported Type 2A and 2B structures solved from a single sample aggregated in PBS at pH 7.4, the major polymorph (83%) was 2A. In our first sample prepared at pH 5.8, we observed 3B as a major polymorph (> 90%) with 3C as a minor polymorph. We hypothesized that the absence of a "3A" polymorph and the presence of the 3B as the major polymorph could be related to the ionic strength of the buffer used in aggregation. Therefore, we also pursued cryo-EM structures under similar conditions but with an additional 50 mM or 100 mM NaCl. While we did see a difference in the relative abundance of the 3B and 3C polymorphs in these samples (Table 1), "3A" was never detected nor was there an obvious correlation between the NaCl concentration and the 3B:3C polymorph population. In fact, in a second sample prepared under the same original PBS conditions which had yielded an approximately 93%:7% 3B:3C ratio, we encountered yet another ratio of 54%:46%, leading us to the conclusion that stochastic or not well-controlled conditions affect the selection between the 'B' and 'C' interface variants of Type 3 fibrils.

Previous reports of non-acetylated α-Syn fibrils seeded from MSA patient material and grown at pH 6.5[26] contained a mixture of 2A, 2B, 3B, and 3C polymorphs as well as hybrid 2/3B fibrils. It is therefore noteworthy that in the five independent amyloid samples that we prepared at pH 5.8, none of them contained a detectable level of Type 2 fibrils. However, in the sample prepared at pH 6.5, we did indeed see a mixture of Type 2 and 3 (2A:2B:3B:3C at 25%:18%:31%:26%) suggesting that Type 2 is not accessible below pH 6 (Figure 5). The structural basis for the Type 3 preference at lower pH may lie in the protonation state of Glu residues in the vicinity of the C-terminal β-strand (i.e. Glu83) or of His50, two regions where polymorphs 2 and 3 are most distinct from each other (discussed below). The fact that we observe the same set of polymorphs in the absence of MSA seed material suggests that not only was the seeding described above non-polymorph specific but also that pH was the main polymorph determinant. Seeding experiments have also been performed with cerebrospinal fluid (CSF) of Parkinson's disease patients at pH 6.5, but this time with N-terminally acetylated α-Syn, and they also produced the 3B and 3C polymorphs[34].

In both the MSA and Parkinson's-CSF seeding experiments, the authors also reported on some samples that produced Type 1-like polymorphs which, unlike most *in vitro* polymorphs, existed primarily as single monomeric fibrils. These are noteworthy because the large majority of *in vitro* and *in vivo* α-Syn polymorphs are composed of more than one protofibril, most often with a C2 or pseudo-C2 helical symmetry. Therefore, we were surprised to find that in one of several pH 7.0 aggregation samples, we also observed a Type 1 monomeric fibril polymorph (termed 1_M), similar to those from the MSA and Parkinsons-CSF seeding experiments and very similar to the Juvenile-onset synucleinopathy (JOS) polymorph[26,41,42] (Figure 6, discussed below). This again indicates that seeding experiments may be influenced by environment-dictated polymorph formation. Also puzzling to us is that we could not produce Type 2 polymorphs at pH 7.0 or 7.5 despite previous reports of 2a and 2b being formed under these conditions[19,27]. In yet another of the pH 7.0 aggregation samples we found a completely new polymorph which we have termed Type 5 (Figure 7). Apart from its novel fold, it is unusual in the number of residues that are visible/ordered in the structure, starting from the acetylated N-terminal methionine (buried at the dimer interface) up until residue 96. Interestingly in a recent BioRxiv manuscript[42] (for which the coordinates are currently on hold), this (or highly

similar) polymorph is found upon seeding with MSA and PD material again indicating that the environment rather than the seeds is responsible for the selection of polymorphs.[14]

In the original reports of Type 2 structures (2A and 2B), fibrils were formed by non-acetylated α-Syn at pH 7.5 in Tris buffer as well by three other constructs at pH 7.0-7.3 in DPBS: (i) the E46K mutant, (ii) phosphorylation at S129 and (iii) an N-terminally acetylated α-Syn. Therefore, we were somewhat surprised that after measuring cryo-EM data for six independent (Table 1) fibrilization samples at pH 7.0 and 7.4 in PBS or Tris, we could not detect any Type 2 polymorphs. Instead, we found that at pH 7.0 in PBS, the samples exhibited a multitude of polymorphs including one having mostly flat (not twisted) fibrils of variable width and the other two each yielding a new polymorph (5A and 1_M). However, in Tris buffer at pH 7.0 we did produce polymorph 1A as the major species. Considering the strong temperature dependence of the Tris pKa, it is worth noting that our Tris buffer was prepared for pH 7.0 at the fibrillization temperature of 37 °C. Returning to PBS but at pH 7.4, polymorph 1A was the dominant species in all three samples that we prepared, including one seeded by 5% Type 3 fibrils that had grown at pH 5.8 (the latter discussed in more detail below). While in our hands 1A is the preferred polymorph above pH 7.0, regardless of the buffer used, we also observed a higher degree of sample variability in the samples grown at pH 7.0 and 7.4. Several samples contained predominantly non-twisted fibrils and could therefore not be used for helical reconstruction. In most samples, we also observed fibrils that were thinner or wider than the known polymorphs, but these were not pursued due to a poor homogeneity between fibrils, lack of twist, or an insufficient number of specimens and so were excluded either during manual picking or later in 2D and 3D classification.

On the structural heterogeneity of Type 1 polymorphs

27 structures of Type 1 polymorphs have been reported, mostly in the pH range of 7.0-7.4 in distinct buffers including Tris or phosphate and comprised of full-length α-Syn, N-acetylated α-Syn, shorter constructs (i.e. 1-103, 1-122), familial mutants (i.e. A53T, A53E, H50Q, and a seven residue insertion associated with JOS), patient-derived material (i.e. MSA and JOS), and fibrils that were seeded by MSA, PD, and dementia with Lewy bodies material (including brain or cerebrospinal fluid). The Type 1 polymorphs display a large structural heterogeneity both at the tertiary structure level (Figure 8) as well as the quaternary level, having distinct protofilament interfaces or even existing as a monomeric fibril. This can be rationalized in part, for example with the familial mutants A53T, A53E, and H50Q which all have been found in polymorph 1C with its smaller protofilament interface (residues 59-60) compared to 1A (residues 50-57). The mutants lie at the 1A interface, destabilizing it and favoring the smaller interface of 1C or even the monomeric 1_M (illustrated in Figure 2). In the context of how buffer conditions influence the polymorph structure, it is interesting to mention that in the presence of phosphate, the Lys58 side chain is often facing out towards the 1A protofilament interface, thereby forming a triad with Lys43 and Lys45 of the other protofilament to surround some extra density that is interpreted to be phosphate (Figure 8). This constellation of Lys residues is found in about 2/3 of the dozen structures of amyloids grown in the presence of phosphate. In contrast, in phosphate-free conditions (such as Tris, PIPES, or unbuffered) Lys58 is facing into the core in about 2/3 of a dozen structures, forming a salt bridge/hydrogen bond with Glu61. Since under both in the presence or absence of phosphate both Lys58 orientations have been documented, other buffer details such as pH may be relevant for this, and other variations. Furthermore, it points to a rather shallow amyloid energy hypersurface that can be altered by subtle changes in the environment.

In the context of polymorph 1 and the interfacial Lys triad discussed above is the structure of the disease-relevant JOS brain-derived polymorph. Here the 1A protofilament interface is disrupted by an additional β-strand comprising the N-terminal residues Gly12-Gly25, yielding a monomeric protofilament structure called Type 1_M (in addition, a double protofilament structure was also observed with a unique protofilament interface). Evidently, the Lys triad of 1A is lost (with Lys58 still facing outward), but now Lys43 and Lys45 together with Lys21 and Lys23 of the N-terminal additional β-strand embrace a small molecule that is likely negatively

charged, yielding overall a similar local structural arrangement around Lys43 and Lys45 (and His50).

In contrast to the brain-derived material, *in vitro* amyloid formation of a mixture of wild-type α-Syn and variant containing the JOS-associated seven-residue insertion MAAAEKT after residue 22 yielded polymorph 1A structures with the typical protofilament interface[33], and not the disease-relevant polymorph. However, in our structure-buffer relationship screening, a JOS-like 1_M polymorph containing the additional N-terminal strand of the JOS polymorph was obtained with wild-type N-terminally acetylated α-Syn. Only with slight changes in the conditions going from pH 7.4 to pH 7.0 in PBS, this polymorph appeared, again illustrating the shallow energy surface between the polymorphs and the critical role of the buffer conditions in polymorph selection. The *in vitro* prepared JOS-like 1_M polymorph superimposes with the Juvenile-onset synucleinopathy purified material almost entirely except for the aforementioned Lys58 side chain facing inward in the former and outward in the latter, and the unassigned peptide density in the latter. The cryo-EM map for the JOS-like 1_M fibrils also has an additional sausage-like density, likely for a beta-strand, but it was not used for model building because it lacked enough features (Figure 6).

On the structural heterogeneity of Type 2 and 3 structures

The structures of Type 2 and 3 polymorphs share some similarities, however, there are significant differences that justify unique polymorph names. First, there is a displacement of the structural fragment comprising residues V52-T72 which appears to move on the G51 and G73 hinges. The turn with residues G73-A78 is again similar between the two structures but beyond this, there is an "inside-out" rearrangement of the C-terminal β-strand (A85-G86-S87-I88-A89-A90-A91-T92) such that only in the Type 2 polymorph can the N-terminal fragment (V15-K21) form an additional β-strand packed against the β-strand A85-A91[19]. However, also within Type 2 and 3 polymorphs exists a large structural heterogeneity: some polymorph 3 structures have an "inside-out" C-terminal β-strand but still without the N-terminal fragment present.

The interfaces present in the 2A and 3C polymorphs also appear to be similar at first glance, consisting of a pair of symmetric salt bridges arranged to create a large solvent-filled cavity at the interface. However, a close inspection reveals that they are different, comprising neighboring sets of E/K residues: K45/E57 in 2A and E46/K58 in 3C. This is remarkable because there is no obvious reason that the "C" interface is preferred over the "A" interface. An example of a 3A polymorph has been reported but it is in the context of the E46K mutant[20] and formed in an unbuffered solution. The familial Parkinson's disease mutant α-Syn (E46K)[46] has been extensively studied and the structures of fibrils of this mutant have been reported at pH 7.5 in Tris[15], at pH 7.4 in PBS[19] and without buffer in 15 mM tetrabutylphosphonium bromide[20]. The Tris condition produced a Type 4 polymorph, the PBS a Type 2A, and the unbuffered condition a Type 3A. Interestingly, since the 2A and 3A polymorphs share the same dimer interface with symmetric K45/E57 salt bridges it is clear that the "A" interface is not mutually exclusive with the Type 3 polymorph. However, it is still not clear as to why Type 3B and 3C polymorphs, both with Glu46 in their salt-bridged dimer interfaces, are preferred for the wild-type protein but we suspected that it was only through the elimination of Glu46 that the E46K mutant could access the 3A polymorph. To test this further, we produced E46K fibrils at pH 5.8, the condition where until now only Type 3 has been observed and uncovered yet another Type 3 polymorph with a new interface termed 3D formed by an E57/K58 salt bridge. This was surprising and suggests that the Type 3 fibrils formed at pH 5.8 are somehow distinct from those formed, until now only by mutants, above pH 7. While researching deposited α-Syn structures we found another Type 3D polymorph (PDB entry 7wo0) that has yet to be published. This other 3D polymorph is formed by the A53T mutant in the presence of 20 mM $CaCl_2$ at pH 7.6. Finally, the coexistence of polymorphs 2A/2B and 3B/3C at pH 6.5 indicates either a similar thermodynamic stability of these polymorphs or a kinetic entrapment. A recent report of two distinct polymorphs grown in a single condition (10 mM Tris, 0.02% NaN_3, pH 7.0 at 37 °C) indicates the latter[47] and considering the temperature dependence of

Tris, the pH might have been close to 6.5 for that study, the same pH where polymorphs 2 and 3 are found to coexist.

The Type 5 structure

Apart from its novel fold, polymorph 5A is unusual in the number of residues that are visible/ordered in the structure, starting from the acetylated N-terminal methionine (buried at the dimer interface) up until residue Lys96. As is often the case, there are shared structural motifs between Type 5 and other α-Syn polymorphs. In particular, residues 47-72, comprising a two-beta strand motif with a turn in between, overlay very well with the polymorph formed by a Tyr39 phosphorylated α-Syn[14] and to a lesser extent in Types 2, 3, and 4 as well. However, the first 35 residues are distinct in that they are usually disordered (Types 1 and 3), or only a segment thereof binds to the core in Type 2 or polymorph 1_M. Within this segment, there are seven Lys and five Glu/Asp residues of which 5 Lys residues are buried inside the structure and form salt bridges with buried Glu/Asp residues. This yields two large cavities separated only by the very polar segment G31-K32-T33-K34-E35-G36, and it is likely that these two cavities are filled with water. In comparison to the other known polymorph structures the cavities and the presence of 5 internal salt bridges are unique. Only polymorph 1 shows a small significant cavity which as discussed above usually appears in the presence of phosphate buffer. Polymorph 5A thus reflects again on the promiscuity of α-Syn polymorph formation, the influence of slight changes in buffer conditions, and more specifically the potential central role of Lys residues in α-Syn's chameleon-like behavior.

The buffer environment dictates the polymorph type also in seeding experiments

The results presented thus far opened an avenue to investigate the polymorph selectivity and mechanism of α-Syn seeding. While for many amyloids, seeded growth results in replication of the structural polymorph of the seeds, the seeding with MSA brain-derived fibrils failed to reproduce an MSA polymorph[26]. Since the MSA polymorphs comprise an unknown molecule, this failure of polymorph-specific seeding could be explained by a missing cofactor. However, as we have observed the buffer environment/condition may play such an important role in polymorph selection, we wondered whether, for pure *in vitro* seeding experiments with *in vitro*-derived seeds, it would be the environment or the seed which dictates the resulting polymorph. To address this, we used seeds of polymorph 3B/3C produced at pH 5.8 in seeding experiments at both pH 7.4 and as a control at pH 5.8. The inverse experiment was also carried out with seeds of Type 1 polymorph produced at pH 7.4 used to accelerate fibril formation both at pH 5.8 and at pH 7.4. For these analyses, we monitored the effect of seeding on the kinetics of fibril formation using Thioflavin T (Thio-T) fluorescence[48,49] and probed the structures of the resulting seeded fibrils by cryo-EM.

Regardless of the conditions, seeding always accelerated the aggregation of α-Syn (Figure 9A). The Cryo-EM results are clear that while pH 7.4 seeds can accelerate the production of fibrils at pH 5.8, only the polymorphs 3B and 3C are obtained (Figure 9B). The inverse is true in that aggregation at pH 7.4 with pH 5.8 seeds produces only polymorph 1A (Figure 9B). We were unable to detect any traces of the seed polymorphs in either of the cross-seeded aggregations despite the fact that 5% seeds were used. Limited proteolysis-coupled mass spectrometry (LiP-MS)[50,51] a quantitative bulk technique that enables the detection of nearly single residue resolution structural differences/alterations in proteins confirmed these findings (data not shown). These data are a clear statement of the fact that polymorph selection under our conditions is governed by the buffer environment and not by the structure of the seed.

Amyloid aggregation can be accelerated by two seed-based processes: (i) fibril elongation and (ii) secondary nucleation. In fibril elongation, the incoming protein adopts the conformation of the seed by attaching itself to the end of the fibril, consequently elongating the fibril. In this process of growth acceleration, which is proportional to the number of fibril ends, the polymorph structure is expected to be preserved[52,53]. In the secondary nucleation process, *de novo* aggregation occurs on the sides of the fibril and therefore the kinetics of secondary nucleation is proportional to the mass of the fibril[54]. In the case of α-Syn, the secondary

nucleation mechanism is based on the interaction of the positively charged N-terminal region of monomeric α-Syn and the disordered, negatively charged C-terminal region of the α-Syn amyloid fibrils[43]. The interaction is transient but causes a further unfolding of the monomeric α-Syn while increasing its local concentration and possibly aligning it in a way that promotes aggregation. Since all known amyloid polymorphs of α-Syn are disordered in their C-terminal regions (residues 100-140) secondary nucleation is proposed to be polymorph unspecific. Our results therefore confirm those of Peduzzo et al.[44] who showed that at lower seed concentrations under which secondary nucleation dominates over fibril elongation, the environment dictates the resulting polymorph.

In addition to the α-Syn seeding experiments discussed until now, Strohäcker et al.[41] used NMR to analyze the results of PMCA using both PD and MSA seed material in PBS buffer at pH 7.4 in the presence of 1% triton X-100. Both samples yielded indistinguishable polymorphs. Hence, it appears that their protocol amplified the seeds via secondary nucleation for which a single polymorph can be expected and whose identity is dependent on the environment; here that includes 1% triton X-100 and 5% w/v brain homogenate. In another PMCA study that is published currently only on the BioRxiv server, Burger et al.[42], use both MSA and PD patient-derived material to produce a new polymorph which they name Type 6. The same Type 6 fold was obtained irrespective of whether the starting material was from an MSA or PD patient brain. Interestingly, the Type 6 fold strongly resembles the Type 5 that we found at pH 7.0, deviating however in its three different dimer interfaces yielding polymorphs 6A, 6B, and 6C. Without the deposited coordinates for the Type 6 structures, it is difficult to ascertain how similar their polymorphs are to Type 5; however, their obvious similarity suggests that the environment of the PMCA seeding and not the identity of the seeds played a large if not the only role in determining the amplified polymorph. Here the environment includes the brain homogenate at 2% w/v and the PMCA buffer: 150 mM KCl, 50 mM Tris, pH 7.5[42] at 37 °C, which considering the temperature dependence of the Tris pK_a could actually be close to pH 7 and thus similar to the buffer conditions that produced Type 5. However, it must also be stated that in contrast to this high-resolution cryo-EM data[42], cell biological and biochemical support for polymorph-specific seeding of the MSA and PD patient-derived material under the same buffer conditions given has been previously found[55].

Considering the importance of reproducing the disease-relevant polymorphs it is apparent that approaches need to be found that can restore PMCA as a tool for α-Syn polymorph-specific amplification. We propose that any approach that reduces or eliminates secondary nucleation is worth pursuing. This could be potentially achieved by using more alkaline fibrillation conditions and higher salt concentration[43] where secondary nucleation appears to be less prominent[56]. The importance of salt for seeded polymorph replication has also been reported for the polymorph-specific seed replication between the non-ThT-sensitive ribbon polymorph and a fibril polymorph that succeeds in 150 mM KCl (with 50 mM Tris, pH 7.5, 37 °C) but not in the absence of KCl[45]. Another approach would be to use an N-terminal-truncated version of α-Syn or to proteolytically remove the disordered C-terminus from the seeds. While it has been shown that with a larger proportion of seeds, it is possible to drive the growth by elongation instead of secondary nucleation[44,45], this may be difficult to achieve by starting from *in vivo* material due to limited sample amounts. Finally, the use of molecules that inhibit secondary nucleation by binding to the C-terminus of α-Syn such as the protein Brichos could be explored.

Conclusion

The presented study primarily on the pH-dependence of fibril polymorph formation as well as cross seeding studies shows the complexity of the fibril formation process, yielding many distinct polymorphs whose diversity is attributed to the absence of an evolutionary selection towards aggregation. On the other hand, it also highlights a rationale for the influence of the environment on this chameleon-like property of alpha-synuclein. With respect to disease, the *in vitro* generation of a JOS-like polymorph could be obtained, and the problem of polymorph-

unspecific seeding could be attributed to secondary nucleation opening an avenue to resolve this open problem in cell and animal disease studies and diagnosis.

Methods

Recombinant protein expression and purification of α-Syn

Recombinant N-terminally acetylated, human WT α-Syn was produced by co-expressing the pRK172 plasmid with the yeast N-acetyltransferase complex B (NatB)[57] in *E. coli* BL21(DE3*). α-Syn was expressed and purified according to the previously published protocol[58] with slight modification. In brief, a single colony from the overnight transformed plate was picked up. It was grown at 37 °C in 100 ml LB media containing 100 µg/ml Ampicillin and 50 µg/ml chloramphenicol. Overnight primary growth culture was added to freshly prepared 1 lit LB media at a final concentration of 2.5% (v/v) containing 100 µg/ml Ampicillin and 50 µg/ml chloramphenicol. It was further grown till O.D reached 0.8. Protein overexpression was initiated by adding IPTG at a final concentration of 1 mM. Thereafter, cells were grown at 37 °C for more than 4 hours and harvested. α-Syn was obtained from a periplasmic extract using a non-denaturing protocol. Finally, pure α-Syn was obtained by ion exchange chromatography followed by purification on a hydrophobic HiPrep phenyl FF 16/10 column (Cytiva). The pure protein was dialyzed extensively against water, lyophilized, and stored at -20 °C until further use.

Amyloid aggregation

Lyophilized α-Syn was dissolved in PBS buffer prepared from commercially available tablets (Sigma-Aldrich). The pH of the dissolved α-Syn was adjusted to pH 7.4 and then separated from aggregates on a Superdex 75 10/60 column (Cytiva) pre-equilibrated with the same buffer and pH. Monomeric α-Syn obtained from SEC was free from any preformed aggregates and its concentration was adjusted to 300 µM. 500 µl of the protein solution was incubated in a 1.5 ml Eppendorf Protein LoBind tube at gentle agitation via tumbling (~50 rpm) at 37 °C for 5 days. The fibrils formed in different pH/buffer conditions were prepared by buffer exchanging the monomeric α-Syn (the elution from the Superdex 75 column) over a PD-10 desalting column (Cytiva) pre-equilibrated in the appropriate buffer and/or pH before incubation at 37 °C with agitation. During every fibrillization procedure, protein concentration and incubated volume were kept constant at 300 µM and 500 µl, respectively, to ensure that different starting conditions do not affect the aggregation process. Similarly, the seeded and cross-seeded fibrils were produced by incubating 300 µM, 500 µl monomeric α-Syn in the presence of 5% (v/v) preformed fibrils (from a previous aggregation of 300 µM α-Syn).

α-Syn aggregation kinetics monitored by ThT fluorescence

α-Syn aggregation kinetics in the presence and absence of preformed seeds was monitored by ThT fluorescence. Monomeric α-Syn prepared and incubated as above and at regular time intervals, 5 µl of the sample was taken and diluted to 200 µl by in the same aggregation buffer. ThT was added at a final concentration of 10 µM and its fluorescence was measured by excitation at 450 nm, and emission at 480 nm with a 5 nm bandpass for both excitation and emission on a Fluoromax-4 (Jobin Yvon) spectrofluorometer. ThT fluorescence intensity at 480 nm was plotted against different time points and three independent measurements were performed for each sample. Here, only 1% of preformed aggregates were used as seeds for ThT measurement in contrast to 5% used for producing fibrils for structural studies.

Electron microscopy grid preparation and data collection

Cu R2/2 300 mesh or Au R2/2 300 mesh grids (Quantifoils) were glow discharged at 25 mA for 30 sec and 120 sec, respectively. Freshly glow-discharged grids were used in a Vitrobot Mark IV (Thermo Fisher Scientific) with its chamber set at 100% humidity and at a temperature of 22 °C. Fibrils (4 uL aliquots) were applied to the grid and blotted for 8 to 15 seconds after a

30-60 second wait time, and subsequently plunge-frozen into a liquid Ethane/Propane mix. The grids were clipped and immediately used or stored in liquid nitrogen dewar.

Data acquisition was performed on a Titan Krios (Thermo Fisher Scientific) operating at 300 kV equipped with a Gatan Imaging Filter (GIF) with a 20 eV energy slit using Gatan's K3 direct electron detector in counting mode. Movies were collected using EPU software (Thermo Fisher Scientific) at a magnification of 130kx (see Table 1 for physical pixel size) and a dose rate of approximately 8 e/pix/sec and total dose ca. 62-74 e/Å^2 (see Table 2 for details).

Image processing

Image processing and helical reconstruction were carried out with RELION 4.0, following the procedure for amyloid structures described by Scheres[59]. RELION's own motion correction was used to correct for drift and dose-weighting and CTF estimation was done using Ctffind4.1[60]. Individual filaments were manually selected, and segments were extracted in a 333 Å box with an inter-box distance of 33 Å and binned 4x to a pixel size of 2.6 Å for initial 2D classification. In the case of mixed polymorphs, larger box sizes were also used to help visually separate the classes and extract the crossover distances. We then used *relion_helix_inidmod2d* to generate an initial model that could be used for the subsequent 3D refinement steps.

Model building and refinement

Models were built into the RELION post-processed maps with ModelAngelo[61] the output of which was manually adjusted in COOT[62] and further adjusted by real-space refinement as a 5 layer fibril in ISOLDE[63]. Figures were prepared with CCP4MG[64] and UCSF Chimera[65].

Acknowledgements
We would like to thank the staff at the ScopeM ETHZ for assistance with the cryo-EM data-collection analysis.

Table 1: Cryo-EM samples analyzed for this manuscript

Construct	Aggregation Condition	pH[3]	Polymorph(s)	Relative abundance[4]
Ac-1-140[1]	PBS[2]	5.8	3B:3C	93%:7%
Ac-1-140	PBS	5.8	3B:3C	54%:46%
Ac-1-140	PBS + 50 mM NaCl	5.8	3B:3C	47%:53%
Ac-1-140	PBS + 100 mM NaCl	5.8	3B:3C	52%:48%
Ac-1-140 (E46K)	PBS + 50 mM NaCl	5.8	3D	
Ac-1-140	PBS	6.5	2A:2B:3B:3C	25%:18%:31%:26%
Ac-1-140	20 mM Tris, 140 mM NaCl	7.0	1A	
Ac-1-140	PBS	7.0	1_M	
Ac-1-140	PBS	7.0	5A	
Ac-1-140	PBS	7.0	flat ribbon[5]	
Ac-1-140	PBS	7.4	1A	
Ac-1-140	PBS + 5% pH 5.8 seeds	7.4	1A	
Ac-1-140	PBS + 5% pH 7.4 seeds	5.8	3B:3C	52%:48%

[1] All constructs are full-length, N-terminally acetylated (Ac)
[2] PBS is a 10 mM phosphate buffer solution with 137 mM NaCl and 2.7 mM KCl
[3] The pH was adjusted after dissolving the PBS tablet (Sigma-Aldrich) by the addition of HCl
[4] In samples for which more than one polymorph could be identified by 3D-classification
[5] This data could not be analyzed by helical reconstruction as only non-twisted fibrils were present

Table 2: Cryo-EM structure determination statistics

Polymorph	1_M	3B	3C	5A	3D (E46K)
Data Collection					
Pixel size [Å]	1.30	0.65	1.30	1.30	0.65
Defocus Range [µm]	-0.8 to -2.5	-0.8 to -2.5	-0.8 to -2.5	-0.8 to -2.5	-0.8 to -2.5
Voltage [kV]	300	300	300	300	300
Number of frames	40	40	40	40	40
Total dose [e- /Å^2]	69	40	67	75	65
Reconstruction					
Reconstruction Box width [pixels]	256	512	256	256	512
Inter-box distance [Å]	33	33	33	33	33
Micrographs	1,164	7,729	3,127	1,850	4,666
Initially extracted segments	84,666	279,929	159,308	109,817	287,018
Segments after 2D and 3D classification	69,283	178,710	28,022	64,476	40,181
Resolution after 3D refinement	3.58	2.87	3.41	3.54	2.40
Final resolution [Å]	3.47	2.68	3.41	3.40	2.31
Estimated map sharpening B-factor [Å^2]	-86.4	-94.4	-101.7	-101.3	-32.8
Helical rise [Å]	4.76	2.37	4.77	4.74	2.38
Helical twist [°]	-0.95	179.5	-0.995	-0.85	179.5
PDB code	8PK2	8PIC	8PIX	8PK4	8PJO
EMDB-ID	17723	17680	17693	17726	17714

Bibliography

1. Chiti, F. & Dobson, C. M. Protein misfolding, functional amyloid, and human disease. *Annual Review of Biochemistry* vol. 75 Preprint at (2006).

2. Meier, B. H., Riek, R. & Böckmann, A. Emerging Structural Understanding of Amyloid Fibrils by Solid-State NMR. *Trends in Biochemical Sciences* vol. 42 Preprint at (2017).

3. He, S. & Scheres, S. H. W. Helical reconstruction in RELION. *J Struct Biol* **198**, (2017).

4. Iadanza, M. G., Jackson, M. P., Hewitt, E. W., Ranson, N. A. & Radford, S. E. A new era for understanding amyloid structures and disease. *Nature Reviews Molecular Cell Biology* vol. 19 Preprint at (2018).

5. Sawaya, M. R., Hughes, M. P., Rodriguez, J. A., Riek, R. & Eisenberg, D. S. The expanding amyloid family: Structure, stability, function, and pathogenesis. *Cell* vol. 184 Preprint at (2021).

6. Riek, R. & Eisenberg, D. S. The activities of amyloids from a structural perspective. *Nature* vol. 539 Preprint at (2016).

7. Törnquist, M. *et al.* Secondary nucleation in amyloid formation. *Chemical Communications* **54**, (2018).

8. Landrieu, I., Dupré, E., Sinnaeve, D., El Hajjar, L. & Smet-Nocca, C. Deciphering the Structure and Formation of Amyloids in Neurodegenerative Diseases With Chemical Biology Tools. *Frontiers in Chemistry* vol. 10 Preprint at (2022).

9. Shi, Y. *et al.* Structure-based classification of tauopathies. *Nature* **598**, (2021).

10. Stahlberg, H. & Riek, R. Structural strains of misfolded tau protein define different diseases. *Nature* vol. 598 Preprint at (2021).

11. Li, Y. *et al.* Amyloid fibril structure of α-synuclein determined by cryo-electron microscopy. *Cell Res* **28**, (2018).

12. Li, B. *et al.* Cryo-EM of full-length α-synuclein reveals fibril polymorphs with a common structural kernel. *Nat Commun* **9**, (2018).

13. Guerrero-Ferreira, R. *et al.* Cryo-EM structure of alpha-synuclein fibrils. *Elife* **7**, e36402 (2018).

14. Zhao, K. *et al.* Parkinson's disease-related phosphorylation at Tyr39 rearranges α-synuclein amyloid fibril structure revealed by cryo-EM. *Proc Natl Acad Sci U S A* **117**, (2020).

15. Zhao, K. *et al.* Parkinson's disease associated mutation E46K of α-synuclein triggers the formation of a distinct fibril structure. *Nat Commun* **11**, (2020).

16. Sun, Y. *et al.* Cryo-EM structure of full-length α-synuclein amyloid fibril with Parkinson's disease familial A53T mutation. *Cell Research* vol. 30 Preprint at (2020).

17. Ni, X., McGlinchey, R. P., Jiang, J. & Lee, J. C. Structural Insights into α-Synuclein Fibril Polymorphism: Effects of Parkinson's Disease-Related C-Terminal Truncations. *J Mol Biol* **431**, (2019).

18. Boyer, D. R. *et al.* Structures of fibrils formed by α-synuclein hereditary disease mutant H50Q reveal new polymorphs. *Nat Struct Mol Biol* **26**, (2019).

19. Guerrero-Ferreira, R. *et al.* Two new polymorphic structures of human full-length alpha-synuclein fibrils solved by cryo-electron microscopy. *Elife* **8**, (2019).

20. Boyer, D. R. *et al.* The α-synuclein hereditary mutation E46K unlocks a more stable, pathogenic fibril structure. *Proc Natl Acad Sci U S A* **117**, (2020).

21. Schweighauser, M. *et al.* Structures of α-synuclein filaments from multiple system atrophy. *Nature* **585**, (2020).

22. Long, H. *et al.* Wild-type α-synuclein inherits the structure and exacerbated neuropathology of E46K mutant fibril strain by cross-seeding. *Proceedings of the National Academy of Sciences* **118**, e2012435118 (2021).

23. Sun, Y. *et al.* The hereditary mutation G51D unlocks a distinct fibril strain transmissible to wild-type α-synuclein. *Nat Commun* **12**, (2021).

24. Hojjatian, A. *et al.* Distinct cryo-EM Structure of α-synuclein Filaments derived by Tau. *bioRxiv* (2021).

25. McGlinchey, R. P., Ni, X., Shadish, J. A., Jiang, J. & Lee, J. C. The N terminus of α-synuclein dictates fibril formation. *Proceedings of the National Academy of Sciences* **118**, e2023487118 (2021).

26. Lövestam, S. *et al.* Seeded assembly in vitro does not replicate the structures of α-synuclein filaments from multiple system atrophy. *FEBS Open Bio* **11**, (2021).

27. Frieg, B. *et al.* α-Synuclein polymorphism determines oligodendroglial dysfunction. *bioRxiv* (2021).

28. Sun, C. *et al.* Cryo-EM structure of amyloid fibril formed by α-synuclein hereditary A53E mutation reveals a distinct protofilament interface. *Journal of Biological Chemistry* (2023).

29. Zhao, Q. *et al.* Structural Insights of Fe3+ Induced α-synuclein Fibrillation in Parkinson's Disease. *J Mol Biol* **435**, (2023).

30. Zhang, S. *et al.* Conformational Dynamics of an α-Synuclein Fibril upon Receptor Binding Revealed by Insensitive Nuclei Enhanced by Polarization Transfer-Based Solid-State Nuclear Magnetic Resonance and Cryo-Electron Microscopy. *J Am Chem Soc* **145**, (2023).

31. Yang, Y. *et al.* Structures of α-synuclein filaments from human brains with Lewy pathology. *Nature* **610**, (2022).

32. Frieg, B. *et al.* The 3D structure of lipidic fibrils of α-synuclein. *Nat Commun* **13**, (2022).

33. Yang, Y. *et al.* New SNCA mutation and structures of α-synuclein filaments from juvenile-onset synucleinopathy. *Acta Neuropathol* (2023).

34. Fan, Y. *et al.* Conformational change of α-synuclein fibrils in cerebrospinal fluid from different clinical phases of Parkinson's disease. *Structure* **31**, (2023).

35. Prusiner, S. B. Prions. in *Proceedings of the National Academy of Sciences of the United States of America* vol. 95 (1998).

36. Aguzzi, A. & Rajendran, L. The Transcellular Spread of Cytosolic Amyloids, Prions, and Prionoids. *Neuron* vol. 64 Preprint at (2009).

37. Saborio, G. P., Permanne, B. & Soto, C. Sensitive detection of pathological prion protein by cyclic amplification of protein misfolding. *Nature* **411**, (2001).

38. Soto, C., Saborio, G. P. & Anderes, L. Cyclic amplification of protein misfolding: Application to prion-related disorders and beyond. *Trends in Neurosciences* vol. 25 Preprint at (2002).

39. Srivastava, A., Alam, P. & Caughey, B. RT-QuIC and Related Assays for Detecting and Quantifying Prion-like Pathological Seeds of α-Synuclein. *Biomolecules* vol. 12 Preprint at (2022).

40. Gerez, J. A. & Riek, R. Neurodegenerative diseases distinguished through protein-structure analysis. *Nature* vol. 578 Preprint at (2020).

41. Strohäker, T. *et al.* Structural heterogeneity of α-synuclein fibrils amplified from patient brain extracts. *Nat Commun* **10**, (2019).

42. Burger, D., Fenyi, A., Bousset, L., Stahlberg, H. & Melki, R. Cryo-EM structure of alpha-synuclein fibrils amplified by PMCA from PD and MSA patient brains. *bioRxiv* (2021).

43. Kumari, P. *et al.* Structural insights into α-synuclein monomer–fibril interactions. *Proc Natl Acad Sci U S A* **118**, (2021).

44. Peduzzo, A., Linse, S. & Buell, A. K. The Properties of α-Synuclein Secondary Nuclei Are Dominated by the Solution Conditions Rather than the Seed Fibril Strain. *ACS Chem Neurosci* **11**, (2020).

45. Bousset, L. *et al.* Structural and functional characterization of two alpha-synuclein strains. *Nat Commun* **4**, (2013).

46. Zarranz, J. J. *et al.* The New Mutation, E46K, of α-Synuclein Causes Parkinson and Lewy Body Dementia. *Ann Neurol* **55**, (2004).

47. Pálmadóttir, T. *et al.* Morphology-Dependent Interactions between α-Synuclein Monomers and Fibrils. *Int J Mol Sci* **24**, (2023).

48. Rogers, D. R. Screening for amyloid with the thioflavin-T fluorescent method. *Am J Clin Pathol* **44**, (1965).

49. LeVine, H. [18] Quantification of β-sheet amyloid fibril structures with thioflavin T. in *Amyloid, Prions, and Other Protein Aggregates* vol. 309 274–284 (Academic Press, 1999).

50. Schopper, S. *et al.* Measuring protein structural changes on a proteome-wide scale using limited proteolysis-coupled mass spectrometry. *Nat Protoc* **12**, (2017).

51. de Souza, N. & Picotti, P. Mass spectrometry analysis of the structural proteome. *Current Opinion in Structural Biology* vol. 60 Preprint at (2020).

52. Jarrett, J. T. & Lansbury, P. T. Seeding 'one-dimensional crystallization' of amyloid: A pathogenic mechanism in Alzheimer's disease and scrapie? *Cell* vol. 73 Preprint at (1993).

53. Jarrett, J. T. & Lansbury, P. T. Amyloid Fibril Formation Requires a Chemically Discriminating Nucleation Event: Studies of an Amyloidogenic Sequence from the Bacterial Protein OsmB. *Biochemistry* **31**, (1992).

54. Knowles, T. P. J. *et al.* Kinetics and thermodynamics of amyloid formation from direct measurements of fluctuations in fibril mass. *Proc Natl Acad Sci U S A* **104**, (2007).

55. Van der Perren, A. *et al.* The structural differences between patient-derived α-synuclein strains dictate characteristics of Parkinson's disease, multiple system atrophy and dementia with Lewy bodies. *Acta Neuropathol* **139**, (2020).

56. Buell, A. K. *et al.* Solution conditions determine the relative importance of nucleation and growth processes in α-synuclein aggregation. *Proceedings of the National Academy of Sciences* **111**, 7671–7676 (2014).

57. Johnson, M., Coulton, A. T., Geeves, M. A. & Mulvihill, D. P. Targeted amino-terminal acetylation of recombinant proteins in E. coli. *PLoS One* **5**, (2010).

58. Campioni, S. *et al.* The presence of an air-water interface affects formation and elongation of α-synuclein fibrils. *J Am Chem Soc* **136**, (2014).

59. Scheres, S. H. W. Amyloid structure determination in RELION-3.1. *Acta Crystallogr D Struct Biol* **76**, (2020).

60. Rohou, A. & Grigorieff, N. CTFFIND4: Fast and accurate defocus estimation from electron micrographs. *J Struct Biol* **192**, (2015).

61. Jamali, K. *et al.* Automated model building and protein identification in cryo-EM maps. *bioRxiv* (2023).

62. Emsley, P. & Cowtan, K. Coot: Model-building tools for molecular graphics. *Acta Crystallogr D Biol Crystallogr* **60**, (2004).

63. Croll, T. I. ISOLDE: A physically realistic environment for model building into low-resolution electron-density maps. *Acta Crystallogr D Struct Biol* **74**, (2018).

64. McNicholas, S., Potterton, E., Wilson, K. S. & Noble, M. E. M. Presenting your structures: The CCP4mg molecular-graphics software. *Acta Crystallogr D Biol Crystallogr* **67**, (2011).

65. Pettersen, E. F. *et al.* UCSF Chimera - A visualization system for exploratory research and analysis. *J Comput Chem* **25**, (2004).

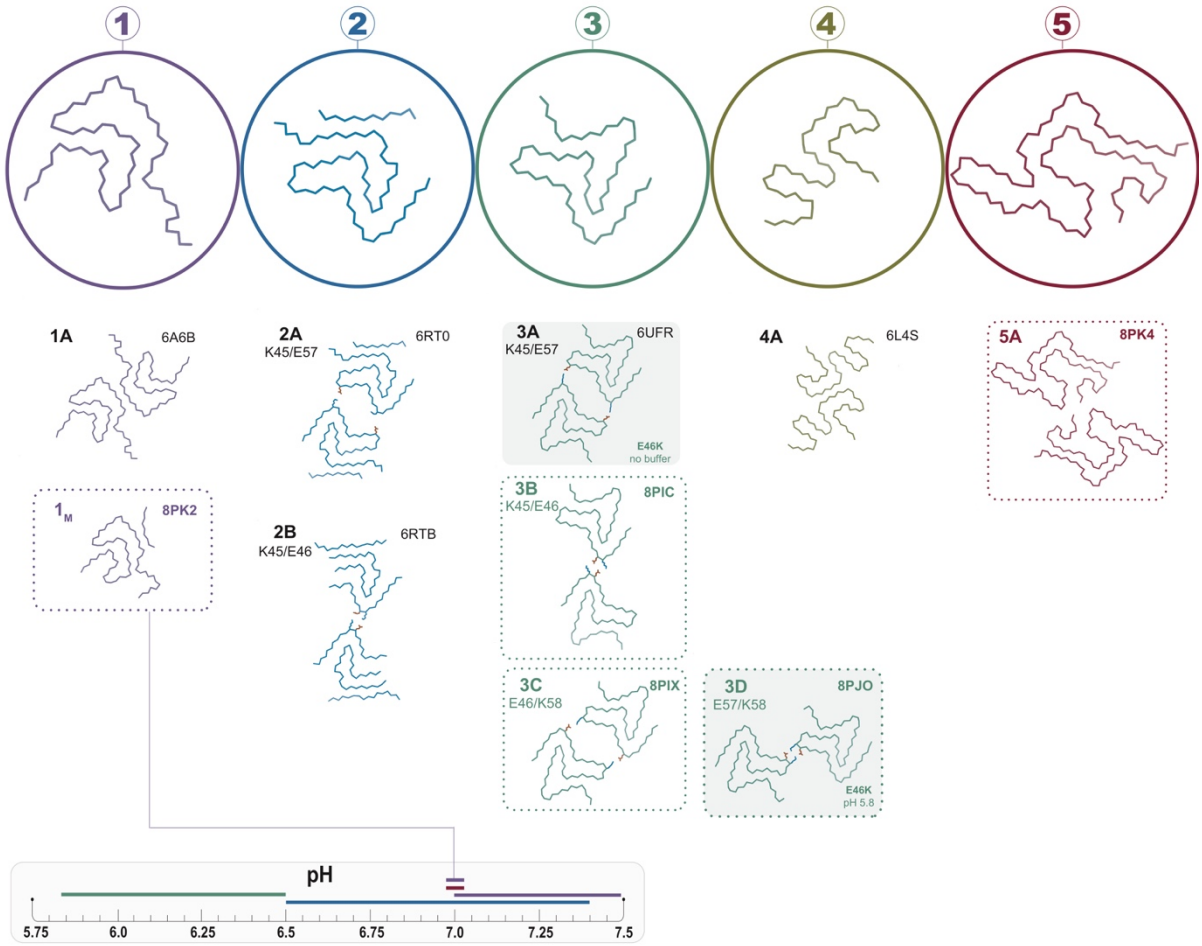

Figure 1. The polymorphs formed *in vitro* by wild-type α-Syn. The numbered backbone Cα traces depicting a single chain from each of the five Types of polymorphs that have been reported to form *in vitro* with wild-type α-Syn but without co-factors. The interface variants of each type are also shown by a representative structure from the PDB or from one of the structures reported in this manuscript (boxed in dotted lines). Two mutant structures for the Type 3 fold are included in order to show the special 3A and 3D interfaces that form for these mutants (shaded background). The pH-dependence of each polymorph is indicated by the colored line above the pH scale (or, in the case of the 1_M polymorph reported here, by a line connecting it to the scale).

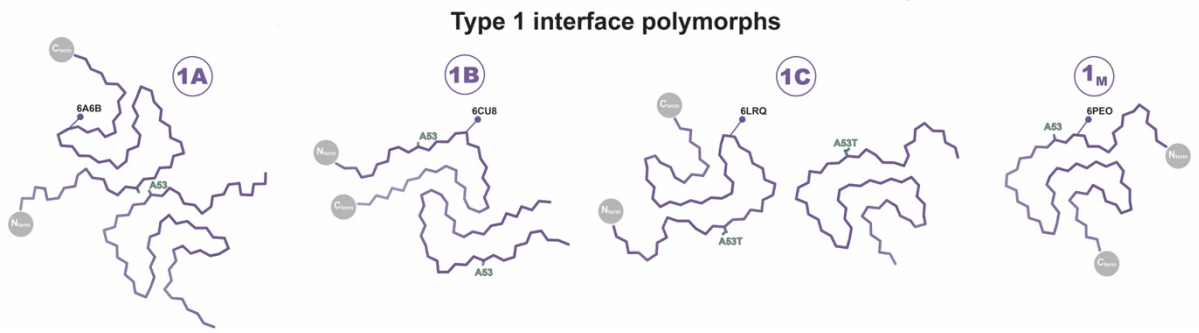

Figure 2. The Type 1 polymorphs. Backbone Cα traces showing the 4 different interface polymorphs of Type 1, including 1B whose fold is not classically Type 1 but whose name is kept for consistency with previous publications. The 1C polymorph is only formed by mutants at the 1A interface (here A53T) and so residue 53 is highlighted in each structure.

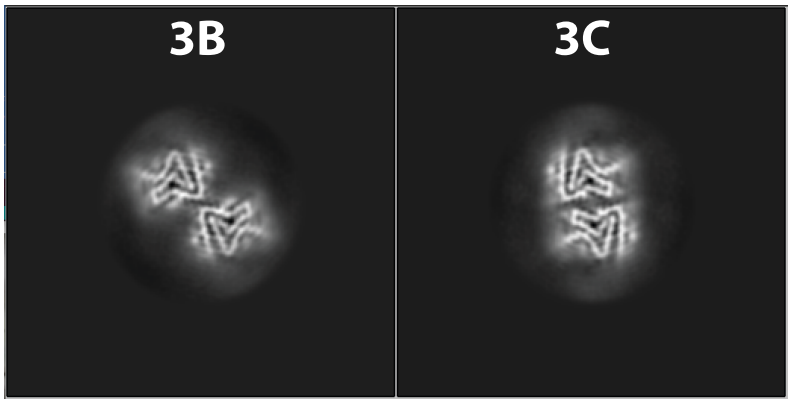

Figure 3. 3D classification of particles in a fibril sample from PBS pH 5.8. A representative 3D-classification in RELION for the fibrils grown at pH 5.8 in PBS showing the 3B and 3C polymorphs. The relative abundance of each polymorph is taken from the ratio of the number of particles assigned to each of the polymorphs.

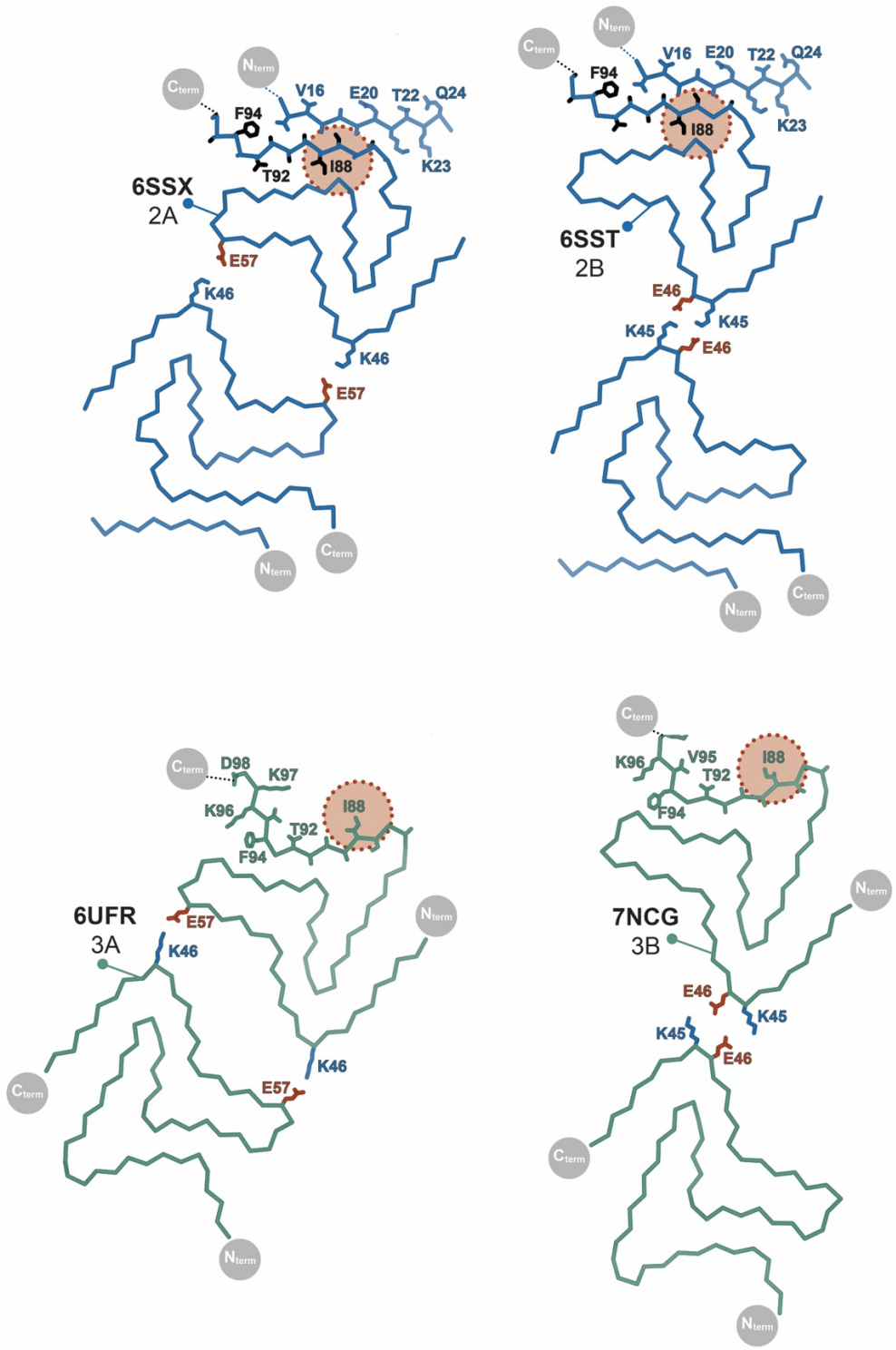

Figure 4. Comparison of the Types 2 and 3 polymorphs. Polymorphs 2A and 2B (blue) and 3B and 3C (green) are depicted, highlighting the change in orientation of the C-terminal β-strand. Residue Ile88 is highlighted to better illustrate how this β-strand flips the inward facing residues to the outside when going from Type 2 to Type 3. Also the N- and C-termini of the peptides are noted to indicate the extra N-terminal β-strand that is bound to the C-terminal β-strand in Type 2.

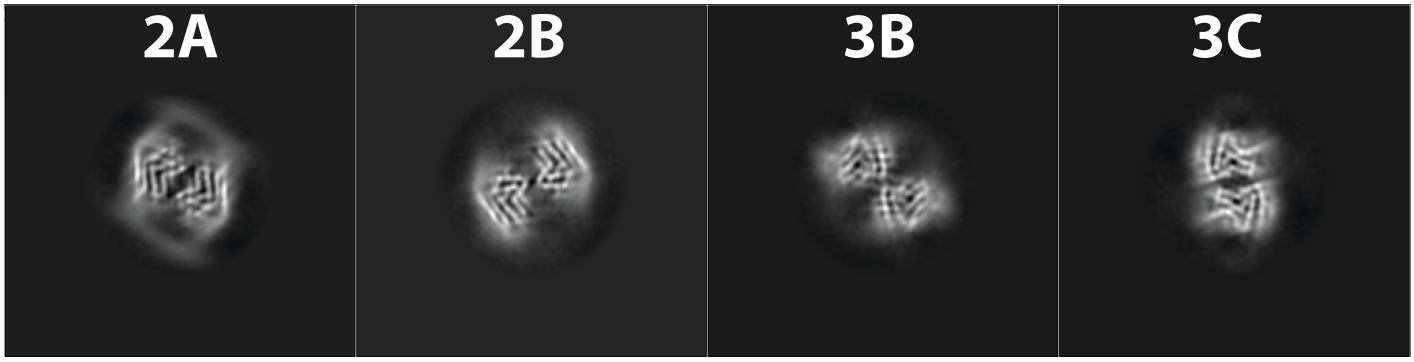

Figure 5. 3D classification of particles in sample from PBS pH 6.5. A representative 3D-classification in RELION for the fibrils grown at pH 6.5 in PBS showing the 2A, 2B, 3B and 3C polymorphs. The relative abundance of each polymorph reported in Table 1 is taken from the ratio of the number of particles assigned to each of the polymorphs from a total of 176,000 particles.

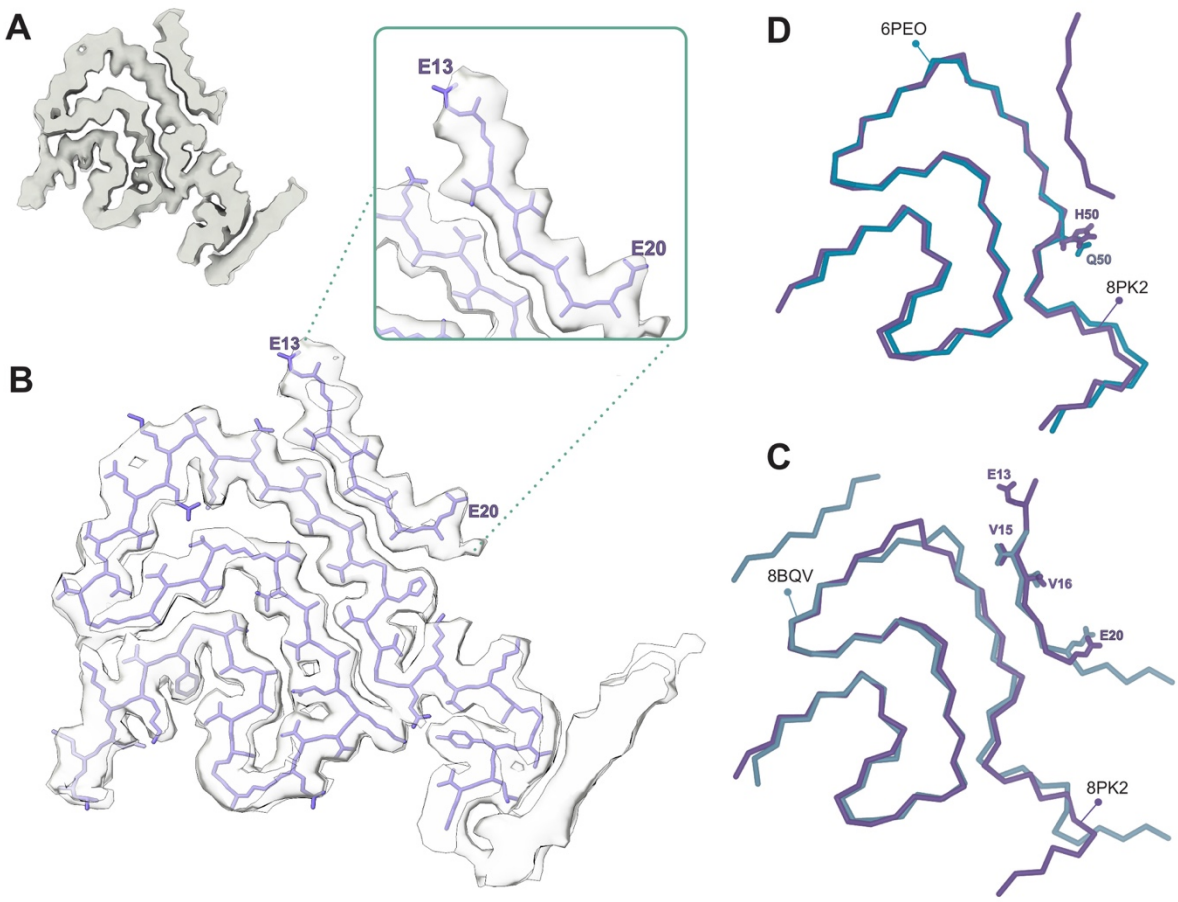

Figure 6. The JOS-like 1_M polymorph. The cryo-EM density map is depicted in **A** and an overlay of the map with the structure (pdb:8PK2) in **B**. The close-up shows the N-terminal β-strand of the novel JOS-like 1_M fold comprising residues 13-20 which binds at the site of the 1A interface. The identity of the residues in the N-terminal strand were taken from an overlay with the JOS polymorph (pdb:8BQV) shown in **C**. The overlay in **D** shows the high similarity of JOS-like 1_M to the 1_M structure of the H50Q mutant (pdb:6PEO).

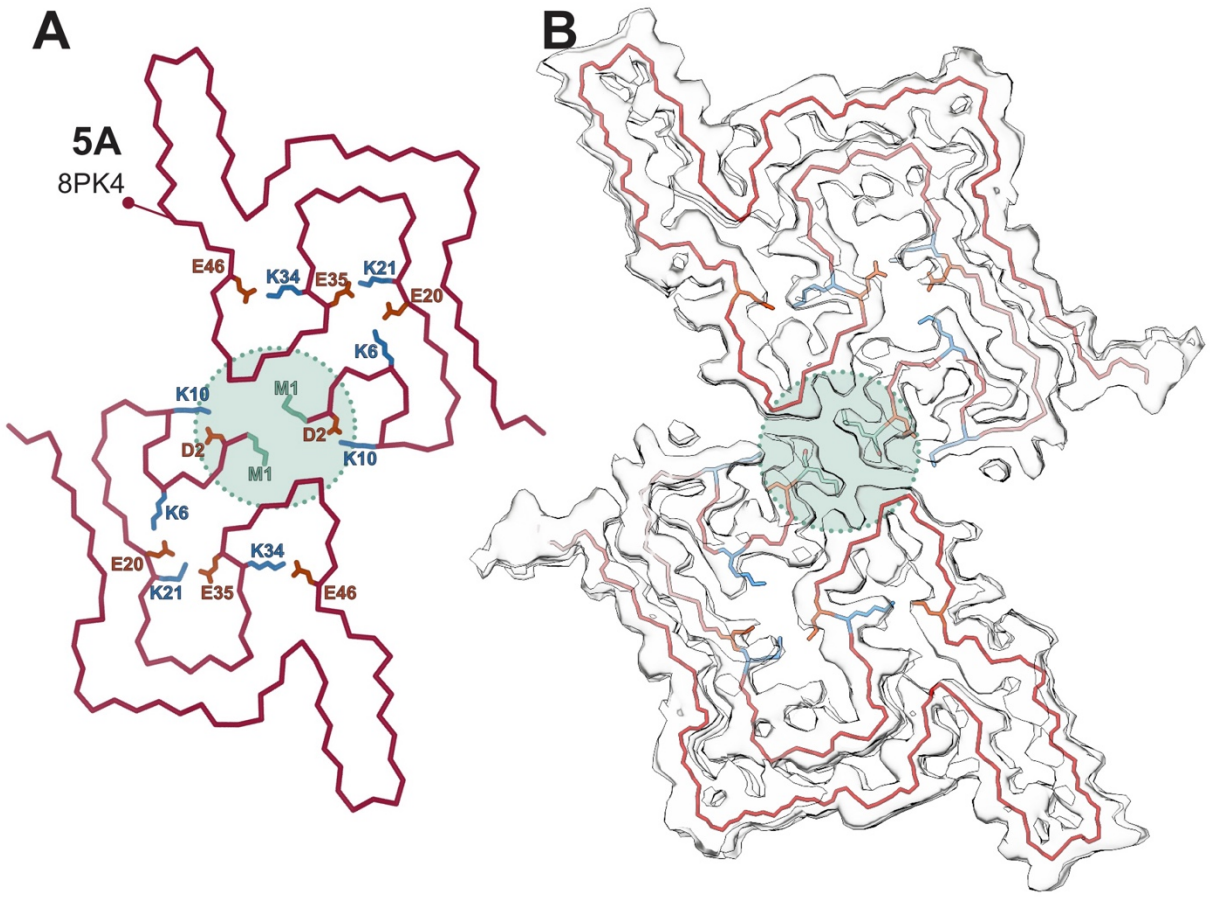

Figure 7. The Type 5 polymorph. The backbone Cα trace of the 5A dimer with the buried Glu and Lys residues highlighted in **A**. The green circle marks the location of the buried acetylated N-terminal methionine. In **B** is the same trace showing the fit to the cryo-EM density map.

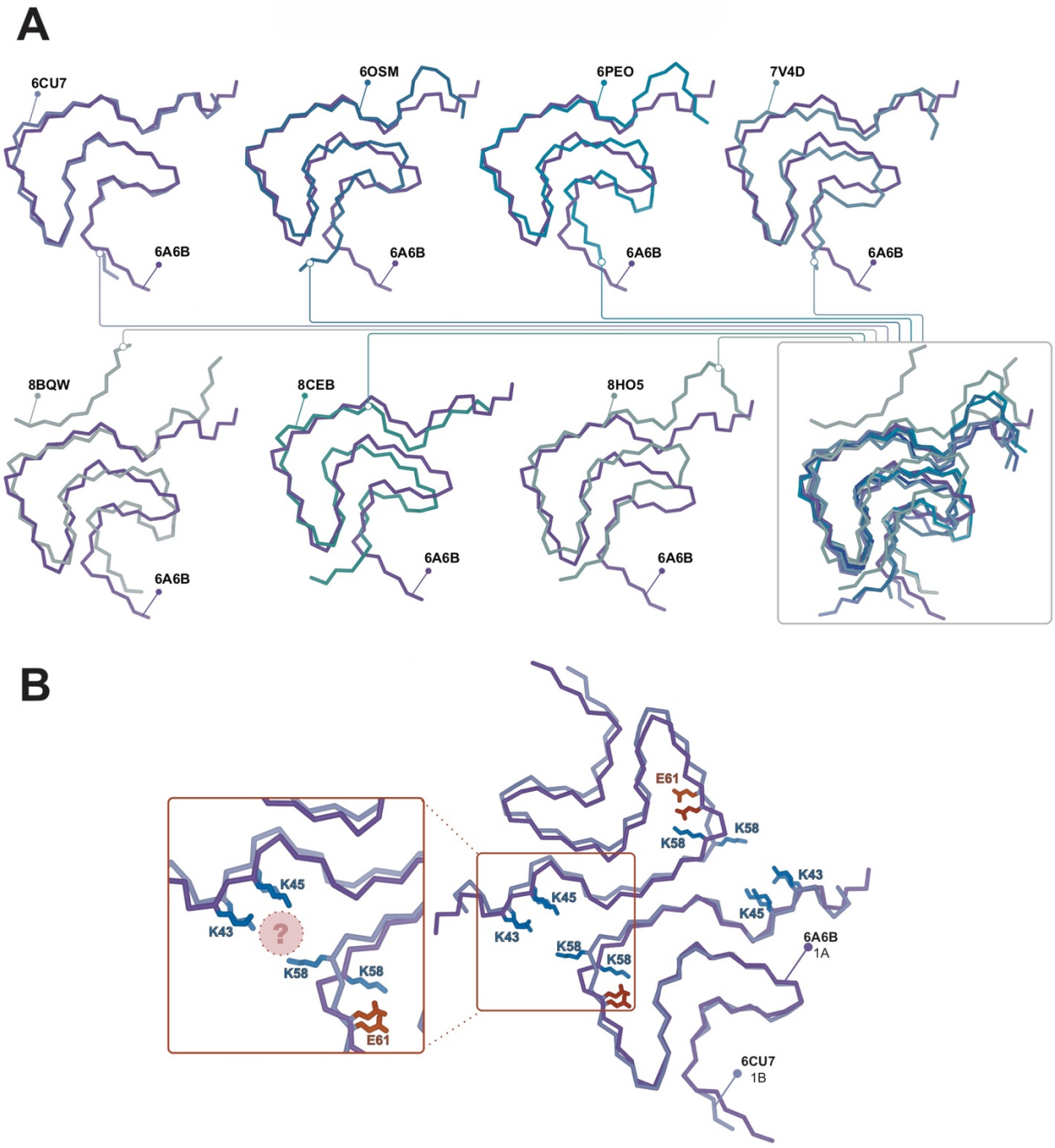

Figure 8. Structural variability within the Type 1 polymorphs. A) Seven pairwise overlays of the wild-type 1A structure (pdb:6A6B) with other wild-type and mutant structures depicting the range of structural variability that is found in the Type 1 fold. The structural alignments were done by an LSQ-superposition of the Cα atoms of residues 51-66. The other Type 1 structures from left to right, top to bottom are wild-type 1A without buffer (pdb:6CU7), N-terminally acetylated wild-type 1A residues 1-103 (pdb:6OSM), the H50Q mutant 1_M without buffer (pdb:6PEO), wild-type 1A in Tris buffered saline (pdb:7V4D), the patient-derived JOS 1_M polymorph (pdb:8BQV), mix of wild-type and seven residue JOS-associated insertion mutant 1A in PBS (pdb:8CEB) and N-terminally acetylated wild-type 1_M seeded from PD patient CSF in PIPES with 500 mM NaCl. **B**) Same overlal shown at the top right in **A**, showing the triad of Lys residues often formed in the presence of phosphate (pdb:6CU7) compared the inward facing orientation of K58 in the absence of phosphate (pdb:6A6B). The location of often observed density, thought to be PO_4^{2-} is indicated with the pink sphere.

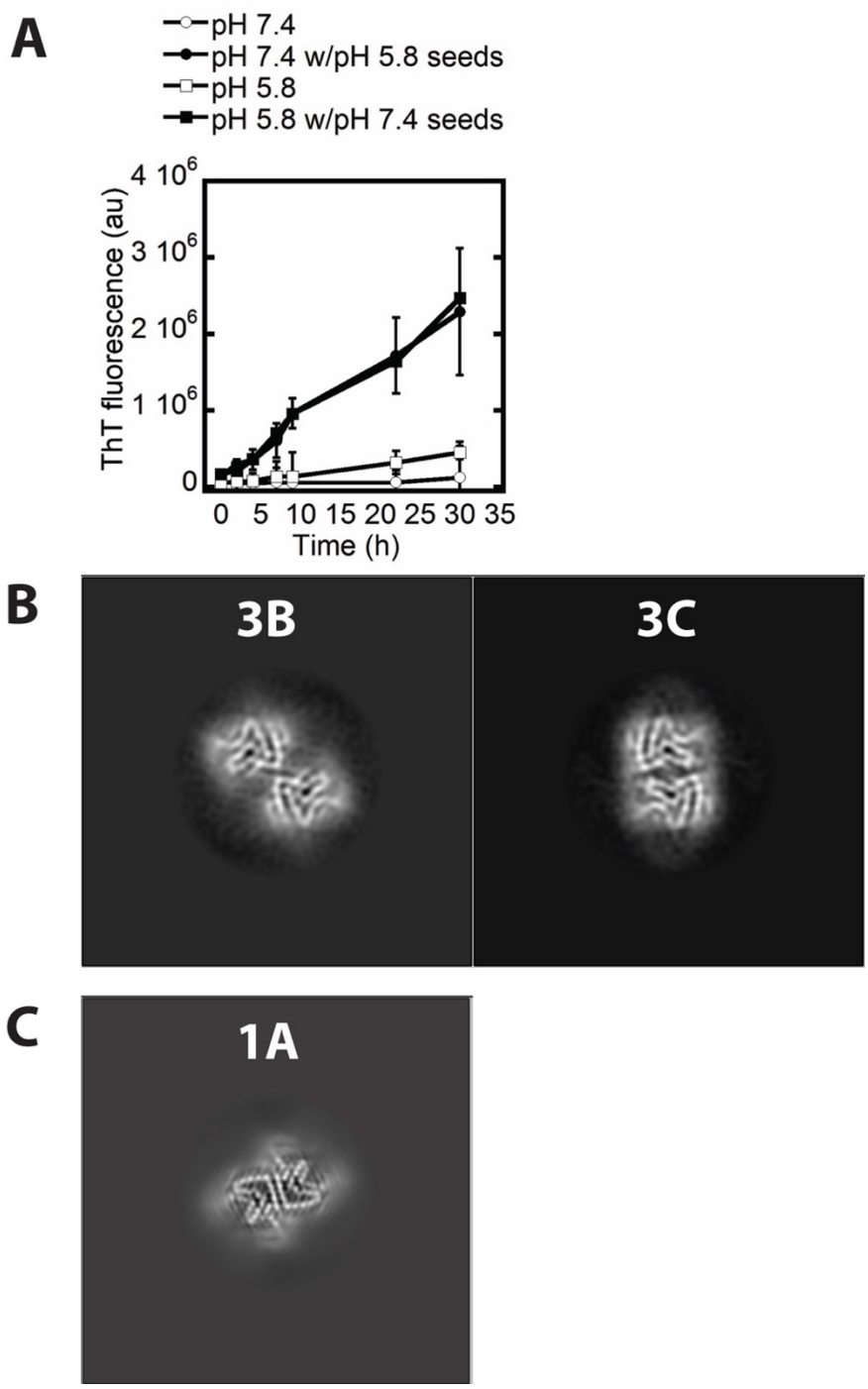

Figure 9. Cross-seeding does not preserve the seed polymorph. A) The effect of cross-seeding with fibrils produced in a different pH from that of the aggregation condition is shown in the aggregations kinetics, as monitored by ThT fluorescence, with and without seeds. **B**) The two 3D classes that were found in the fibrils grown at pH 5.8 and seeded with 5% fibrils from pH 7.4 representing polymorphs 3B and 3C. **C**) The single 3D class that was found in the fibrils grown at pH 7.4 and seeded with 5% fibrils from pH 5.8 representing polymorph 1A.